Interfacial supercooling and the precipitation of hydrohalite in frozen NaCl solutions as seen by X-ray absorption spectroscopy

Thorsten Bartels-Rausch[1], Xiangrui Kong[1*], Fabrizio Orlando[1**], Luca Artiglia[1], Astrid Waldner[1], Thomas Huthwelker[2], Markus Ammann[1]

[1]Laboratory of Environmental Chemistry, Paul Scherrer Institut, Villigen PSI, Switzerland
[2]Swiss Light Source (SLS), Paul Scherrer Institut, Villigen PSI, Switzerland
* now at: Department of Chemistry and Molecular Biology, Atmospheric Science, University of Gothenburg, Gothenburg, Sweden
** now at: Omya International AG, Oftringen, Switzerland

Correspondence to: Thorsten Bartels-Rausch (thorsten.bartels-rausch@psi.ch)

Abstract. Laboratory experiments are presented on the phase change at the surface of sodium chloride – water mixtures at temperatures between 259 K and ~~240~~ 241 K. Chloride is a ubiquitous component of polar coastal surface snow. The chloride embedded in snow is involved in reactions that modify the chemical composition of snow as well as ultimately impact the budget of trace gases and the oxidative capacity of the overlying atmosphere. Multiphase reactions at the snow – air interface have found particular interest in atmospheric science. Undoubtedly, chemical reactions proceed faster in liquids than in solids; but it is currently unclear when such phase changes occur at the interface of snow with air. In the experiments reported here, a high selectivity to the upper few nanometres of the frozen solution – air interface is achieved by using electron yield near-edge X-ray absorption fine structure (NEXAFS) spectroscopy. We find that sodium chloride at the interface of frozen solutions, which mimic sea-salt deposits in snow, remain as supercooled liquid down to ~~240~~ 241 K. ~~Below~~ At this temperature, hydrohalite exclusively precipitates, anhydrous sodium chloride is not detected. In this work, we present the first NEXAFS

27   spectrum of hydrohalite. The hydrohalite is found to be stable while increasing the temperature

28   towards the eutectic temperature of ~~253~~ 252 K. Taken together, this study reveals no differences in

29   the phase changes of sodium chloride at the interface as compared to the bulk. That sodium

30   chloride remains liquid at the interface upon cooling down to ~~240~~ 241 K, which spans the most

31   common temperature range in Polar marine environments, has consequences for interfacial

32   chemistry involving chlorine as well as for any other reactant for which the sodium chloride

33   provides a liquid reservoir at the interface of environmental snow. Implications for the role of

34   surface snow on atmospheric chemistry are discussed.

37   Abstract Teaser

38   **1 Introduction**

39   Chemical cycling of halogens affects the composition of the troposphere and via this effect

40   influences climate and impacts human health (Simpson et al., 2007; Abbatt et al., 2012; Saiz-

41   Lopez and von Glasow, 2012; Simpson et al., 2015). Taken the abundance of chloride in the form

42   of sea-salt over wide areas of the globe, the atmospheric chemistry of chlorine has long raised

43   interest in ~~a number of~~several multiphase reactions that liberate chloride into chlorine species in

44   the gas phase (Simpson et al., 2007; Finlayson-Pitts, 2010). Chlorine has a direct role as a sink for

45   ozone. Further, reactive chlorine species act as a powerful oxidant on atmospheric cycles that

46   destroy or produce ozone and are relevant for the atmospheric oxidation capacity (Finlayson-Pitts,

47   2003; Thornton et al., 2010). Atmospheric ozone is of concern because it directly impacts

48 atmospheric composition, health, and climate (Simpson et al., 2007). Prominent examples of these

49 reactions in the atmosphere with chloride in sea-salt or salt-dust are shown in Fig. 1 and discussed

50 in the following. Acid displacements, where the nitric or sulfuric acid are taken up into the aqueous

51 phase, lead to the emission of hydrochloric acid to the gas phase. Further examples are reactions

52 with OH radicals (Knipping et al., 2000; Halfacre et al., 2019), and with nitrogen oxides (Osthoff

53 et al., 2008). Common to all of these reactions is the generation of chlorine gases that either react

54 with OH radicals or photolyze at wavelengths available in the troposphere to generate reactive

55 chlorine (Fig. 1 and Finlayson-Pitts (2010)). Given their importance, these multiphase reactions

56 have intensively been investigated in laboratory studies over the last decade (Abbatt et al., 2012;

57 Saiz-Lopez and von Glasow, 2012; Simpson et al., 2015). One outcome of these investigations is

58 the importance of reactions at the liquid – air interface as compared to those proceeding in the

59 bulk. An example is the oxidation of chloride by OH radicals. In contrast to the aqueous phase

60 reactions, it does not require the presence of acid to proceed fast at the air—water interface (Laskin

61 et al., 2006).
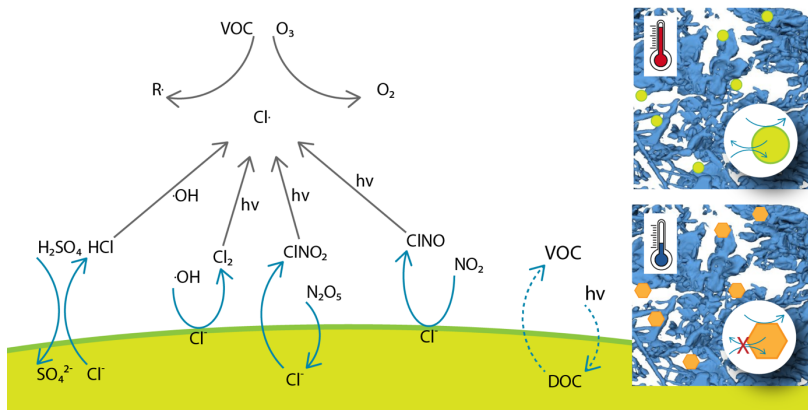
62

63 Figure 1: Simplified scheme of multiphase reactions liberating chlorine from sea-salt deposits to

64 the atmosphere and subsequent reactions of chlorine with impacts on the ozone budget and air

65 quality. These reactions may occur both in the bulk phase and at the air-deposit interface for liquid

66 particles. The sea-salt may also maintain a liquid phase for the reaction of other reactants such as

67 the photolysis of organics. The inserts illustrate sea-salt deposits in snow and how phase changes

68 from solid (orange pentagon) to aqueous solutions (green circle) impact the chemical reactivity.

69 See text for details and references.

70

71 The relevance of halogen multiphase chemistry for the atmosphere is not limited to chlorine. A

72 more recent example is the oxidation of bromide. Bromide is present in sea-salt, is a key reactant in

73 ozone depletions in polar atmospheres (Simpson et al., 2015), and participates in atmospheric

74 chlorine chemistry by forming interhalogen compounds (Finlayson-Pitts, 2003). Oldridge and

75 Abbatt (2011) have shown that a Langmuir-Hinshelwood type surface reaction of ozone with

76 bromide occurs at the liquid – air interface simultaneously with a corresponding bulk reaction in

77 the temperature range of 263 K to 248 K. A surface-active reaction intermediate was found to

78 explain the high interfacial reactivity for the case of the reaction with ozone (Artiglia et al., 2017),

79 while other bromine species may directly exhibit surface propensity on their own (Gladich et al.,

80 2020). Clearly, this line of research shows how reaction kinetics and mechanisms differ at the

81 interface from those in the bulk and that heterogeneous chemistry is a key driver in atmospheric

82 chemistry.

83

84 In the cryosphere, where the snowpack is strongly impacting the chemistry in the overlaying

85 atmosphere (Dominé and Shepson, 2002; Thomas et al., 2019), halogen compounds are also found

86 within the snow. Sea-salt components, a source of halogens in snow in costal snowpack, might

87 originate from migration from underlying sea-ice or from deposition of wind-transported sea-spray

88 aerosol (Dominé et al., 2004). One characteristic of the cryosphere are its subfreezing

89 temperatures and the consequent precipitation of chemical constituents at specific temperatures,

90 their eutectic temperature, as also observed in sea-ice (Petrich and Eicken, 2009). It is known that

91 the precipitations or phase changes of the reactants critically impact the reactivity (Bartels-Rausch

92 et al., 2014; Kahan et al., 2014). Reduced chlorine production in frozen systems was observed by

93 Wren et al. (2013) and by Sjostedt and Abbatt (2008), at temperatures below the eutectic

94   temperature of sodium chloride – water mixtures in laboratory experiments that was attributed to
95   the precipitation of the salt. In an arctic field study, Custard et al. (2017) observed reduced Cl_2
96   production when temperatures dropped and suggested limited availability of chloride as
97   consequence of the precipitation in this surface snow. Further, Lopez-Hilfiker and Thornton (2012)
98   proposed the precipitation of sodium chloride salts to explain the changes in the production yield
99   of $ClNO_2$ from the reaction of N_2O_5 with saline frozen systems with temperature.
100
101   ImportantlyMore generally, it is not only the chlorine chemistry that responds to the phase of
102   sodium chloride present in frozen systems both in the laboratory and in the environment. Oldridge
103   and Abbatt (2011) showed that the rate of the heterogeneous reaction of ozone with bromide in
104   sodium chloride -- water mixtures is strongly reduced once sodium chloridethe chloride salt
105   precipitates below 252 K. The author explained this with the reduction in liquid volume that serves
106   as reaction medium for the bromide in the sample due to the precipitation of sodium chloride.
107   Similar, the photolytical reaction of nitroanisol with pyridine was found to depend on the amount
108   of liquid in frozen samples and thus to critically respond to precipitation of sodium chloride
109   (Grannas et al., 2007). Next to its role in atmospheric halogen chemistry, sodium chloride is thus
110   further of importance as salt to establish and maintain liquid solutions at subfreezing temperature.
111   Its importance arises from its atmospheric abundance but also because its eutectic temperature of
112   252 K falls into typical springtime Arctic temperatures – a region and time period when
113   atmospheric halogen chemistry is most active. For example, at the Arctic coast near Utqiagvik
114   (Alaska) temperatures have been reported to fluctuate between 247 K and 259 K within days
115   (Custard et al., 2017). Another region of Earth's cryosphere, where temperatures drop below 252 K
116   is the troposphere (Thomas et al., 2019). Wang et al. (2015) have proposed a significant role of
117   tropospheric heterogeneous halogen chemistry on the ozone budget there. More recently, Murphy
118   et al. (2019) have shown that the amount of sea-salt aerosol lifted to the upper troposphere is small,
119   casting some doubt on the environmental relevance of sea-salt as matrix for multiphase chemistry
120   there.
121

122 While the phase diagram of sodium chloride – water binary mixtures and the thermodynamic

123 stability domains of salt, solution, and ice are well known (Koop et al., 2000a), the precise

124 occurrence of nucleation and sodium chloride precipitation is still debated (Koop et al., 2000a;

125 Wise et al., 2012; Peckhaus et al., 2016). Figure 2 shows a part of the phase diagram of sodium

126 chloride -- water mixtures and can be used to illustrate the appearance of the individual phases.

127 Below 251.9 K, the eutectic temperature of sodium chloride (Koop et al., 2000a), ~~anhydrous~~ solid

128 sodium chloride dihydrate (hydrohalite, $NaCl \cdot 2H_2O$) ~~(NaCl, halite)~~ and solid water (ice) are the

129 energetically favoured phases. ~~Increasing the temperature of such a hypothetical sample to above~~

130 ~~251.9 K, the sodium chloride will change its phase from solid halite to an aqueous sodium chloride~~

131 ~~solution. Ice remains the second phase at temperatures between 251.9 K and 273.2 K. Above~~

132 ~~273.2 K, the ice will melt completely and an aqueous sodium chloride solution will be the only~~

133 ~~phase present. A characteristic of these systems is that~~ Bbetween the eutectic temperature and ~~the~~

134 ~~melting point of ice, the system moves along~~ the so-called ~~ice stability~~liquidus line~~.~~, ice and

135 sodium chloride solution (brine) co-exist. The ice will melt completely above the liquidus line, and

136 an aqueous sodium chloride solution is the only phase present. The focus of this work was to

137 experimentally observe phase changes of sodium chloride below the eutectic temperature. A

138 typical experimental procedure started with a dry sample of anhydrous sodium chloride (halite,

139 NaCl) which was exposed to increasing gas-phase water at constant temperature of 259 K. ~~More~~

140 ~~general, by~~By absorbing ~~and evaporating~~ water from the surrounding air~~, composition and volume~~

141 ~~of the brine will change. Such changes with varying relative humidity (hygroscopic growth) have~~

142 ~~long been discussed for aerosol in the troposphere. The changes include~~, a ~~phase transitions~~ from

143 the solid salt to ~~the~~ a liquid solution (deliquescence) took place. Upon increasing the gas-phase

144 water dosing further (Fig. 2, red arrow) ice crystallised and a two-phase system of ice and brine

145 occurred (Fig. 2, red cross). After probing the sample at this position in the phase diagram (see

146 below), temperature was lowered and the dosing of the water-vapor adopted to move along the

147 liquidus line to below the eutectic temperature. ~~and from the liquid to the solid (efflorescence) in~~

148 ~~aerosol particles at specific temperature and water partial pressure conditions.~~ ~~,~~During this cooling

149 period, salt ~~composition~~concentration and volume of the brine ~~will~~ changes. Such changes with

varying relative humidity (hygroscopic growth) have long been discussed for aerosol in the troposphere. The changes includeIn other words, the concentration of the sodium chloride in solution changes with temperature to maintain both phases in equilibrium. At the air-ice interface where both phases are in equilibrium with water vapour in the gas phase, this can be understood by considering that the aqueous sodium chloride solution and ice need to have the same vapour pressure. Otherwise, the phase with the higher water vapour pressure would vanish by evaporation and the one with the lower vapour pressure would grow by condensation. The vapour pressure of ice decreases with decreasing temperature while that of an aqueous solution decreases with increasing concentration of solute. With a fixed amount of sodium chloride present in our experiments and also in individual sodium chloride deposits in snow, consequently the amount of liquid is given by temperature (Koop et al., 2000a). More general, by absorbing and evaporating water from the surrounding air, composition and volume of the brine will change. Such changes with varying relative humidity (hygroscopic growth) have long been discussed for aerosol in the troposphere. The changes include phase transitions from the solid to the liquid solution (deliquescence) and from the liquid to the solid (efflorescence) in aerosol particles at specific temperature and water partial pressure conditions. Because relative humidity is such a strong driver of the hygroscopic growth, we base the discussion of phase changes in this work on the relative humidity the sample was exposed to. The relative humidity is a measure of the partial pressure of water relative to the vapour pressure of (supercooled) liquid at the same temperature {Marti, 1993}. An advantage of this experimental approach with environmental relevance is that the relative humidity precisely matches that in the atmosphere in contact and in thermodynamic equilibrium with ice clouds or snow cover, because the relative humidity is a sole function of temperature in the presence of ice. Therefore, the chemical concentration of such particles exactly matches those of same composition in snow or in the atmosphere under environmental conditions.
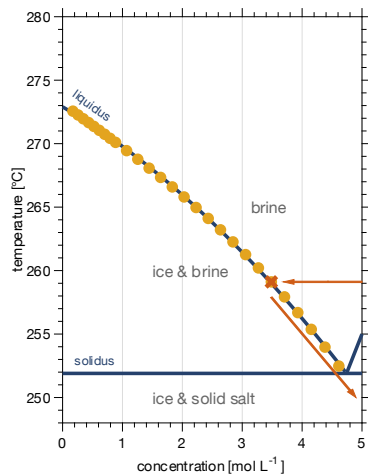
174

175 Figure 2: Phase diagram of the NaCl-water binary system. The data show the freezing point

176 depression of sodium-chloride solutions (yellow filled circles) and give the concentration of an

177 aqueous sodium chloride solution in equilibrium with ~~water~~ ice in the temperature range of 273 K

178 to 254 K (Rumble, 2019). The dark blue lines indicate the phase boundaries (Koop et al., 2000b;

179 Rumble, 2019), that is it denotes the so-called liquidus and solidus line, respectively, and thus

180 shows the temperature and concentration range where ice and aqueous sodium chloride solution

181 co-exist. The eutectic temperature of sodium chloride – water binaries is 251.9 K (Koop et al.,

182 2000a). Also shown is a typical experimental procedure (red arrows and cross).

183

184 Koop et al. (2000a) were the first to show that because precipitation of sodium chloride can be

185 kinetically hindered ~~, i.e. precipitation may not occur even though temperature has dropped below~~

186 ~~the eutectic temperature where the solid is the thermodynamically favoured phase,~~ supercooled

187 sodium chloride solutions in the presence of ice can prevail down to 240 K. Precipitation of

188 sodium chloride may not occur even though temperature has dropped below the eutectic

189 temperature where the solid is the thermodynamically favoured phase. Cho et al. (2002) have

190 observed a liquid fraction in sodium chloride – water mixtures at even lower temperatures of

191 between 228 K and 273 K based on the evaluation of ^{1}H-NMR signals. Cho et al. (2002) proposed

192 the presence of liquid below the eutectic temperature to be an interfacial phenomenon, stabilized

193 by surface forces in analogy to the disordered interface observed for neat ice surfaces when

194 approaching the melting point (Bartels-Rausch et al., 2014).

195

196 The goal of this study is to investigate the precipitation and the occurrence of liquid features in

197 sodium chloride – water binary mixtures in the interfacial region. Both Cho et al. (2002) and Koop

198 et al. (2000a) have applied methods that are not specifically sensitive to the interface, but are

199 probing the bulk. Near Edge X-ray Absorption Fine Structure (NEXAFS) spectroscopy is

200 inherently sensitive to the upper few nanometre of interfaces when detecting electrons as done in

201 this work. Oxygen K-edge NEXAFS spectra of H_2O are an established tool to investigate the

202 hydrogen bonding structure of water and ice with its clear differences for solid and liquid water

203 (Bluhm et al., 2002; Nilsson et al., 2010; Krepelova et al., 2013; Newberg and Bluhm, 2015;

204 Orlando et al., 2016; Bartels-Rausch et al., 2017; Ammann et al., 2018; Waldner et al., 2018). In

205 our earlier NEXAFS study (Krepelova et al., 2010a), it was shown by probing the X-ray absorption

206 of oxygen atoms in sodium chloride – water binary mixtures that the hydrogen bonding network

207 did not reveal the presence of any liquid features at the interface below the eutectic temperature.

208 Interpretation of these oxygen NEXAFS spectra was complicated by the appearance of crystal

209 water in the hydrohalite and by the presence of adsorbed H_2O. Also, the oxygen spectra might be

210 dominated by ice that is present in equilibrium with the sodium chloride solution and thus small

211 fractions of liquid might have been difficult to detect. In this work, we therefore discuss Cl K-edge

212 NEXAFS that have previously been used to inspect the chemical speciation of chlorine in glasses

213 and in coal (Huggins and Huffman, 1995; Evans et al., 2008). Interest in the local environment of

214 chloride at the interface in sodium chloride – water binary mixtures ~~comes~~come also from earlier

215 work on nitric and hydrochloric acid adsorbed at the ice-air interface. We have shown that nitrate

216 and chloride form~~s~~ solvation shells with a hydrogen-bonding structure similar to that in aqueous

217 solution in the interfacial region of ice at concentrations low enough to prevent melting (Krepelova

218 et al., 2010b; Kong et al., 2017). The aim of this study is thus also to investigate the occurrence of

219 solvated chloride at the interface of sodium chloride – water mixtures at temperatures close to the

220 eutectic. Motivation comes from the role of heterogeneous chemistry in atmospheric science in

221 general and in particular on the impact that the microchemical environment has on the reactivity.

222

223 **1 Experimental Part**

224 Experiments were performed at the PHOENIX beam line of the Swiss Light Source (SLS) at the

225 Paul Scherrer Institute using the Near Ambient Pressure Photoemission (NAPP) set-up previously

226 described (Orlando et al., 2016). NAPP is equipped with a differentially-pumped electron analyser

227 (Scienta R4000 HiPP-2). The central feature of NAPP is a flow-through cell with a sample holder

228 the temperature of which is computer-controlled by a flow of cooled helium gas. The

229 measurements were performed with partial pressures of water between 0.3 mbar and 1.8 mbar in

230 the flow-through cell and temperatures of the sample between 259 K and ~~240~~241 K.

231 **1.1 Sample Preparation and Water Dosing**

232 To prepare a sample, 1 µl of a 2.12 g sodium chloride (Fluka Trace Select 38979-25G-F) solution

233 in 80 ml of water (Fluka Trace Select 142100-12-F) was dropped at the centre of the sample holder

234 and dried at 60 °C. The sample holder was then moved into the flow-through cell and kept at UHV

235 and at 60 °C to 80 °C for 45 minutes to remove volatile impurities. Water vapour was dosed to the

236 flow-through cell via a 0.8 mm i.d. steel capillary from the vapour above liquid water (Fluka Trace

237 Select 142100-12-F) in a vacuum-sealed, temperature-controlled glass reservoir. Before dosing, the

238 water was degassed by 4 freeze-pump-thaw cycles. The ~~relative humidity~~water dosing and thus the

239 partial pressure or relative humidity that the sample was exposed to was ~~increased~~varied by

240 ~~increasing~~setting the temperature of the reservoir to change the flux of water vapour into the

241 experimental cell. Pressure in the flow-through cell was monitored by a capacitance manometer

242 (Baratron 626A) with a measurement range from 5×10^{-4} mbar to 10 mbar and an accuracy of

243 0.25 % of the reading. Temperature was monitored with a Pt-1000 sensor located at the edge of the

244 sample holder. The sensor was calibrated prior to the experiments by growing ice on the sample

245 holder and noting its vapour pressure which is a direct measure of the temperature at the sample

246 spot (Marti and Mauersberger, 1993). During the experiments, the calibration was confirmed when

247 ice was present. At 253 K, the offset between temperature reading and calibration was found to be

248 4.3 ± 0.2 K.

249 **1.1 X-ray exited Electron Spectroscopy**

250 Partial Auger-Meitner electron-yield NEXAFS spectra at the Cl K-edge were acquired with a fixed

251 kinetic energy window of 2370 eV to 2390 eV, which includes the KL2,3L2,3 Auger-Meitner peak

252 of chlorine. The pass energy and dwell time were set to 200 eV and 300 ms, respectively. The

253 distance of the sample to the electron analyser inlet (working distance) was 1 mm. ~~and T~~the

254 electron analyser was operated with an electron sampling aperture with a diameter of 500 μm,

255 which results in sampling roughly an area on the icy sample with a diameter of 500 μm from which

256 the emitted electrons reach the detector. NEXAFS spectra were measured by sweeping the

257 incident X-ray photon energy across the chlorine K-edge from 2815 eV to 2845 eV with steps

258 ranging from 0.2 eV to 1 eV. The NEXAFS spectra were processed by dividing by the photon flux

259 (I_0) as derived *in-situ* using a Ni coated membrane, by subtracting the mean pre-edge intensity as

260 background, and by normalising to the mean intensity at 2830 eV to 2833 eV X-ray photon energy.

261 Photoemission spectra (XPS) of O1s, Cl2p, Na1s, C1s, and Au4f were recorded at an incident X-

262 ray photon energy of 2200 eV and ~~a~~ with a pass energy of 100 eV and a dwell time of 120 ms. To

263 quantify, a linear background was ~~applied~~applied, and the photoemission signal was integrated in

264 Matlab without any peak fitting.

265 **1 Results and Discussion**

266 **NEXAFS of brine, halite, and hydrohalite**

267 Figure 3 shows chlorine K-edge X-ray absorption spectra of ~~NaCl~~ sodium chloride salts and of

268 frozen NaCl-water binary mixtures in the presence of ice. This NEXAFS spectroscopy probes the

269 X-ray absorption by chlorine atoms, corresponding to the resonant excitation of core electrons into

270 unoccupied molecular orbitals. As exactly those outer orbitals are forming chemical bonds,

271 NEXAFS spectra directly reflect changes to the local chemical environment and structural

272 arrangement. NEXAFS spectroscopy of halogen salts has thus been used to discuss their phase and

273 chemical speciation in geological examples (Huggins and Huffman, 1995; Evans et al., 2008). In

274 this work, the X-ray absorption spectra were derived by recording the intensity of Auger-Meitner

275 electrons at 2370-2390 eV, which corresponds to the KL2,3L2,3 transition in chlorine (Cleff and

276 Mehlhorn, 1969). Detecting electrons, as done in this work, makes X-ray absorption inherently

277 surface sensitive, because electrons have a limited escape depth in matter (Ammann et al., 2018).

278 The escape depth can be quantified by relating it to the inelastic mean free path (IMFP) of

279 electrons in matter and to the take-off angle of detected electrons relative to the surface normal.

280 The IMFP of electrons with a kinetic energy of 2380 eV is about 7 nm in NaCl and in ice (Tanuma

281 et al., 1991). The take-off angle of electron detection is 30° in our set-up (Orlando et al., 2016),

282 which gives an escape depth of 6 nm, meaning that cumulatively, 95% of the electrons detected

283 originate from 18 nm, with an exponentially decreasing contribution from the surface towards the

284 bulk. In the following, we report the NEXAFS spectra derived from this interfacial region of NaCl-

285 water binary mixtures to discuss changes in the solvation of chloride by water as we explore the

286 regions of the phase diagram where precipitation of sodium chloride has been described for bulk

287 samples.

288

289 All chlorine K-edge spectra show a strong absorption peak at 2825-2830 eV (region I), the

290 absorption edge, corresponding to the transition of electrons from the 1s to the empty 4p orbitals.

291 Halite salt, in Fig. 3 A, shows a strong absorption in region I, and a characteristic feature at

292 2838 eV (region II) (Huggins and Huffman, 1995; Evans et al., 2008). The difference in the
293 relative intensity of region I as compared to the intensity at photon energies > 2830 eV between
294 Fig. 3A and Huggins and Huffmann (1995) comes from the latter using fluorescence as detection
295 mode. Detecting X-ray absorption with fluorescence probes deeper into the bulk of the samples
296 and therefore often suffers from self-absorption which leads to less signal intensities at the
297 absorption edge (region I).
298
299 The small feature at 2821 eV can be assigned to C-Cl bonds that may form in-situ due to reactions
300 involving secondary electrons and organic impurities (Fujimori et al., 2010). The sample
301 composition in the interfacial region was further investigated by X-ray photoemission
302 spectroscopy. The C1s and Cl2p spectra support the presence of C-Cl compounds in the samples
303 (Appendix A): A small feature in the Cl2p spectra at 3 eV higher binding energy than the main
304 chlorine signal might be attributed to organic carbon species. The C1s photoemission spectra show
305 a feature at 1.5 eV higher binding energy than the main feature, typical for C-Cl compounds. The
306 main feature of the C1s photoemission spectra is attributed to C-H bonds, the dominant component
307 of adventitious carbon that forms in a cascade of reactions with secondary electrons during the
308 experiments. A further source of carbon might be omnipresent traces of carbon in the NaCl and
309 introduced when preparing the NaCl samples. The atomic ratio of the total carbon to oxygen from
310 water present at the interface was below 0.25, except for samples in Fig. 3A and F where total
311 carbon to oxygen atomic ratios were 0.5-0.75. Adsorbed water molecules were present at the
312 interface of all samples, and ice or liquid water formed in some samples, as gaseous water was
313 present in all experiments with pressures between 0.3 mbar to 1.8 mbar. The atomic ratio was
314 derived based on the measured C1s/O1s photoemission intensities and a calibration to account for
315 the analyser efficiency and total X-ray photoionization cross section using C1s/O1s photoemission
316 intensities of 0.8 mbar CO_2 gas following a procedure used before (Krepelova et al., 2013). Direct
317 comparison between the individual samples and estimation of surface coverages of the carbon
318 impurities is hampered by the varying water content at the sample's interface as adsorption and
319 water uptake varies with the individual relative humidity settings.

320

322
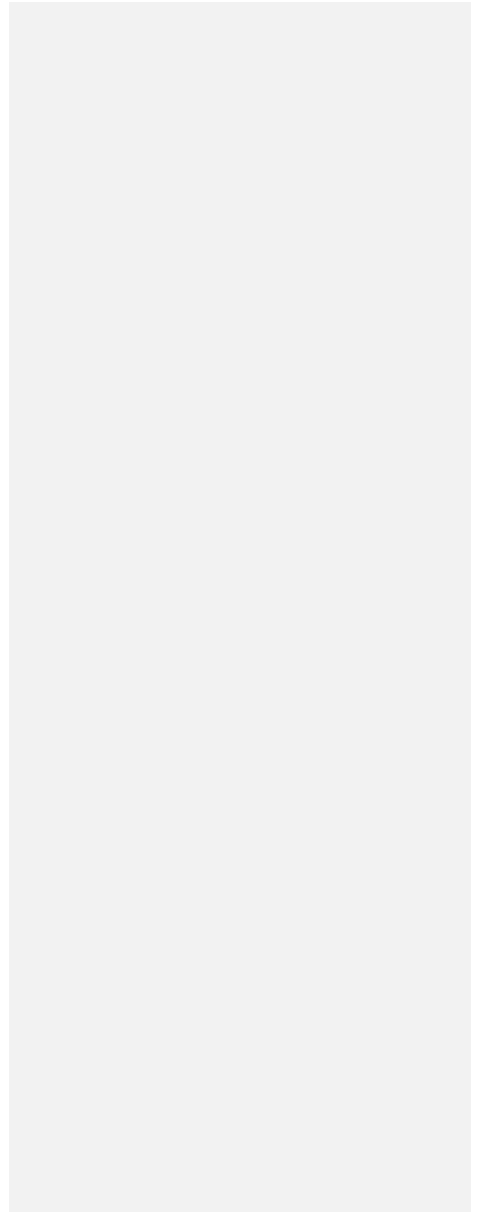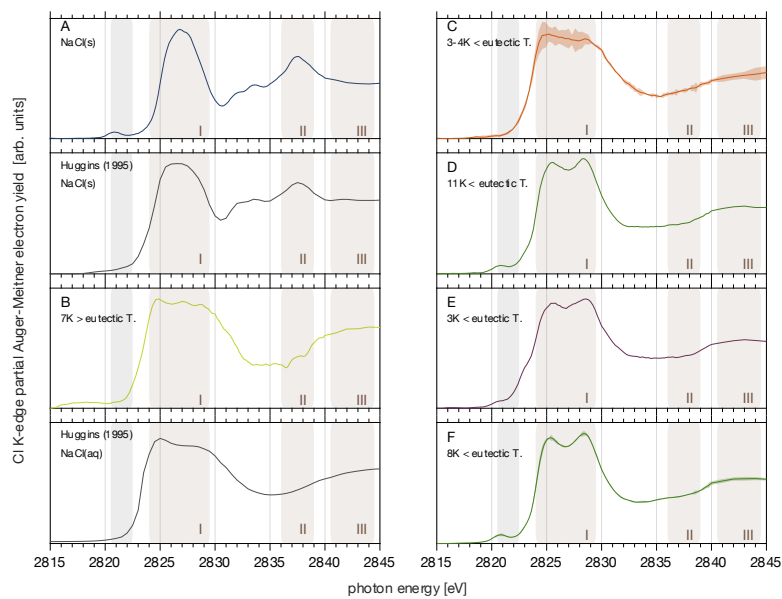
Figure 3: Partial electron yield chlorine K-edge NEXAFS spectra of the sodium chloride -- water binary system: **A** Solid NaCl at 248 K and 44 % relative humidity (0.34 mbar water vapour pressure). **B** Aqueous NaCl solution in equilibrium with ice at 88 % RH (1.82 mbar) and 259 K. **C** An averaged spectrum at the thermodynamic ice stability line at 248 K to 249 K and 78 % (0.60 mbar) to 80 % RH (0.71 mbar). **D** An individual spectrum upon further cooling to 24~~10~~ K and 74 % RH 0.29 mbar). **E** An individual spectrum upon heating back to 249 K in the ice stability domain at 79 % RH (0.69 mbar). **F** The averaged spectrum at 244 K and ~~a relative humidities~~RH of 59 % (0.32 mbar) and 73 % (0.40 mbar), lower than the ice stability domain. See Fig. 4 for precise measurement settings. The shaded area in the colour of the graph in C and F denote the standard deviation of 3 and 2 repeated NEXAFS acquisitions. Also shown are NEXAFS spectra of NaCl salt and aqueous solutions for comparison that were detected in fluorescence mode and not in partial electron yield (Huggins and Huffman, 1995). The brownish shaded area (I-III) highlights regions in the NEXAFS spectra ~~disused~~ discussed in the text. The grey shaded area at 2821 eV highlights the photon energy region where carbon-chlorine bonds from carbon contamination might show an absorption feature (see text for details).

334

335
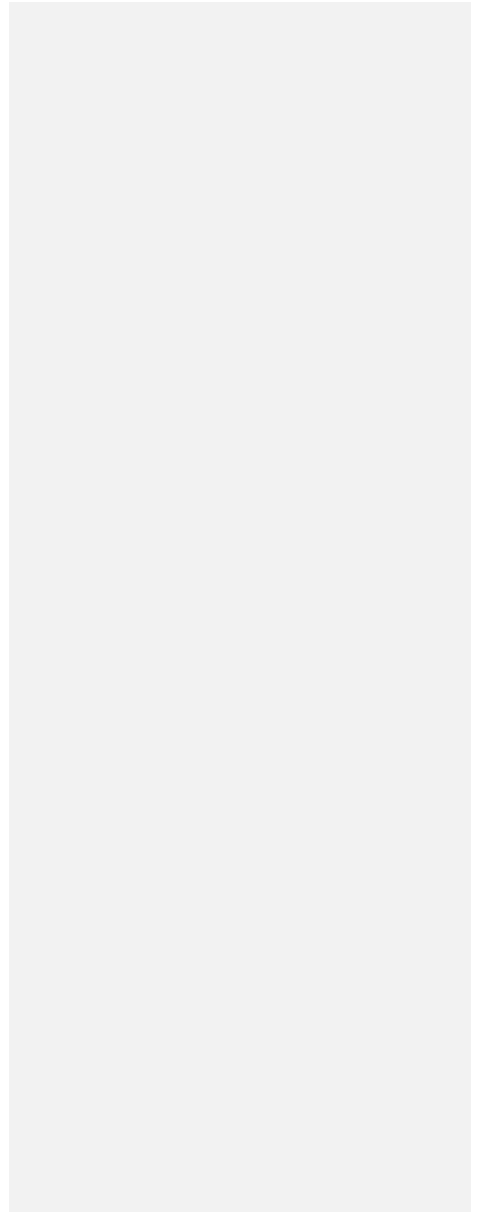
336 The spectrum of sodium chloride in aqueous solution, Fig. 3B, shows a broader absorption peak in
337 region I compared to the spectra of the halite and a second feature at 2840 eV (region III) (Huggins
338 and Huffman, 1995). In this work, the NEXAFS spectrum of NaCl in aqueous solution was
339 recorded in a solution-ice binary mixture based on the phase diagram (see Efflorescence at the
340 Interface). Based on freezing point depression data, the concentration of sodium chloride in such
341 an aqueous solution in equilibrium with ice is 3.5 mol l^{-1} (Rumble, 2019). The spectrum in Fig. 3B
342 generally agrees with the X-ray absorption spectra reported for 0.1 mol l^{-1} and 1 mol l^{-1} aqueous
343 solutions (Fig. 3 Huggins and Huffman (1995)) as it captures the general decrease in intensity in
344 region I with excitation energy and the increase in absorption in region III (Fig. 3). Discussing
345 differences in the hydration structure of chloride at the water—air interface as compared to the
346 bulk solution is beyond the scope of this work. Harada et al. (2011) has reported differences in the
347 hydration structure of Br$^-$ at the aqueous surface compared to in bulk. Due to the low spectrum
348 quality, evident by the wiggles in region I, we refrain from discussing the two distinct features in
349 region I, at 2824 eV and 2829 eV, that have been observed in previous work on NEXAFS spectra
350 of aqueous chloride solution (Huggins and Huffman, 1995; Antalek et al., 2016).
351
352 Figure 3C-~~E~~ E show NEXAFS spectra acquired in the ice stability domain at temperatures below
353 the eutectic temperature of 251.9 K (Koop et al., 2000a). By comparing these spectra to the spectra
354 in Fig. 3 A-B, the phase of the sodium chloride in the presence of ice below the eutectic
355 temperature will be discussed. ~~At~~When cooling to 248-249 K from above the eutectic temperature,
356 the NEXAFS spectrum resembles that of a typical aqueous solution (Fig. 3C). Figure 3C shows an
357 average of 3 individual NEXAFS spectra which still shows substantial scatter that results in low
358 spectra quality. We assign the spectral quality,~~is~~ to the low amount of salt within the interfacial
359 region and to potential thermal circulations and thus redistribution of the liquid upon irradiation by
360 the beam. Despite this uncertainty, the results in Fig. 3A-C allow to clearly differentiate between
361 solid halite and aqueous solution.
362

363   Upon cooling further to 241 K, the spectrum changed significantly. The NEXAFS spectrum in Fig.

364   3D shows a wide peak in region I with two well resolved features about 3 eV apart. That both

365   features have a similar intensity, makes this spectrum clearly distinct from those of an aqueous

366   NaCl solution with its decreasing trend of absorption in region I. Compared to the spectrum of

367   aqueous NaCl solution (Fig. 3B, C), the absorption edge is shifted to higher photon energies in the

368   spectrum in Fig. 3D. The absence of a feature in region II makes the spectrum in Fig. 3D distinct

369   from the spectrum of anhydrous NaCl salt. Notably, the spectrum quality is greatly improved and

370   is similar to that of the solid, anhydrous halite sample (Fig. 3A). One factor impacting the spectral

371   quality is the stability of the sample during the NEXAFS acquisition. The analysis of the Cl 2p

372   photoemission spectra acquired before and after each NEXAFS run showed that the amount of

373   chlorine detected in the sample volume fluctuated by less than 10%, between 0 % and 9 %, in

374   samples shown in Fig. 3 C, D, E, and F (Appendix A). For comparison, samples in Fig. 3 A and B

375   showed a decrease of 39 % and 43 % in the integrated Cl 2p signal intensity, respectively, from

376   prior- to after the NEXAFS was recorded. Possible reasons for these trends are an increase in

377   adsorbed water with time masking the intensity of the underlying chlorine (Fig. 3A) and changes in

378   the distance of the sample to the electron analyser with time leading to a reduction in the intensities

379   of all compounds (Fig. 3 B). ~~Both of these~~Both processes would also affect the NEXAFS signal by

380   inducing changes in intensity with time. Direct quantitative comparison is beyond the scope of this

381   ~~work, and~~work and is hampered by the different probing depth of XPS and NEXAFS as given by

382   the kinetic energy.

383

384   We assign the spectrum in Fig. 3D to that of sodium chloride dihydrate (hydrohalite, $NaCl \cdot 2H_2O$).

385   The NEXAFS spectrum of the hydrohalite has to the best of our knowledge not been described

386   before. The double peak feature in region I, ~~that~~ we observe ~~here~~in this work, is typical for other

387   chloride hydrates such as $MnCl_2 \cdot 4H_2O$, $CaCl_2 \cdot 2H_2O$, and $MgCl_2 \cdot 6H_2O$ (Evans et al., 2008). It is

388   also present in the NEXAFS spectra of sodium chloride solution (Huggins and Huffman, 1995),

389   with a different ratio of the two features as observed here for the hydrohalite. Antalek et al. (2016)

390   has explained this double peak feature in NEXAFS spectra of aqueous chloride solutions by the

391   formation of two distinct solvation shells with two distances between the chloride and the solvating

392   water molecules based on NEXAFS and extended X-ray absorption fine structure spectroscopy as

393   well as molecular dynamics simulations. We propose here that the NEXAFS spectra of the

394   hydrohalite can be understood based on the same argument, as the chloride in NaCl•2H$_2$O is

395   coordinated by two sodium and four water molecules with differences in the distance of each Cl to

396   the neighbouring oxygen of the water molecules (Klewe et al., 1974).

397

398   Figures 3E and 3F shows a hydrohalite spectruma after warming the sample back to 249 K in the

399   presence of ice. Clearly, the observed shape in region I show that hydrohalite and not liquid brine

400   is the dominant phase of this sample. In Fig. 3 F an averaged spectrum and at 244 K in absence of

401   ice is shown, again the shape is in good agreement to spectrum shown in Figure 3D. We'd like to

402   note the excellent reproducibility of the spectra as seen in Fig. 3F by the small standard deviation

403   of two samples (shaded area). In summary, we have clearly presented three different chlorine K-

404   edge NEXAFS spectra and argued that these derive from the halite, chloride solution, and the

405   hydrohalite. Hydrohalite at the air-ice interfacial region was thus observed in the temperature range

406   241 K – 249 K.

407
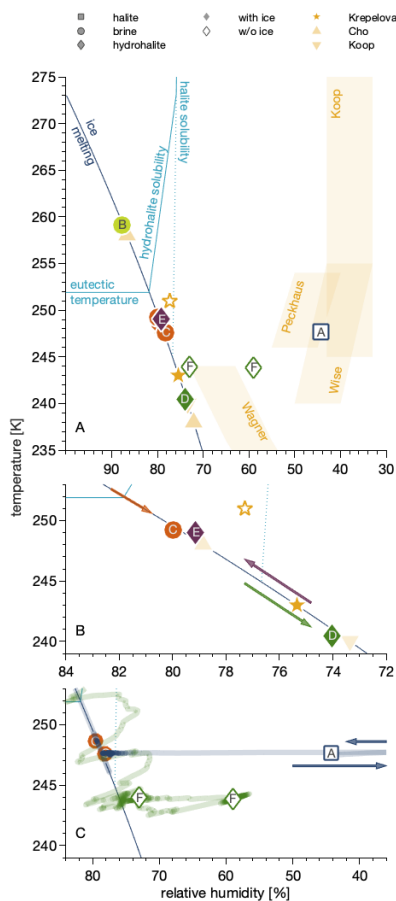
Figure 4: Phase diagram of the NaCl-water binary system showing the conditions and trajectories of the data in Fig. 3 in the relative humidity – temperature space. The relative humidity is the partial pressure of water relative to the vapour pressure of (supercooled) water as parameterised by Marti and Mauersberger (1993). The dark blue line denotes settings where ice is stable as the partial pressure of water matches the vapour pressure of ice. Above the eutectic temperature, it thus separates regions where ice and NaCl solution coexist from those where only NaCl solutions exist. The light blue lines denote conditions where anhydrous NaCl salt ('halite solubility') and where NaCl•2H₂O ('hydrohalite solubility') forms a solution when increasing the relative humidity at constant temperature; and where NaCl•2H₂O dissolves with increasing temperature at constant relative humidity ("eutectic temperature").

A Data from this work compared to previous results. Also shown are the data ranges where efflorescence has been observed in earlier work as shaded areas (Koop et al., 2000a; Wagner et al., 2011; Wise et al., 2012; Peckhaus et al., 2016). **B** Zoom into data below the eutectic temperature. The arrows show the sequence of changes in experimental temperature and relative humidity conditions. **C** Zoom to the data in absence of ice. The lines indicate the relative humidity and temperature trajectories to reach the experimental conditions for these data points. The arrows illustrate that the relative humidity was reduced to 0 % prior to returning to the conditions of the measurement.

438

439

440

441
442
443
444
445
446
447
448
449
450
451
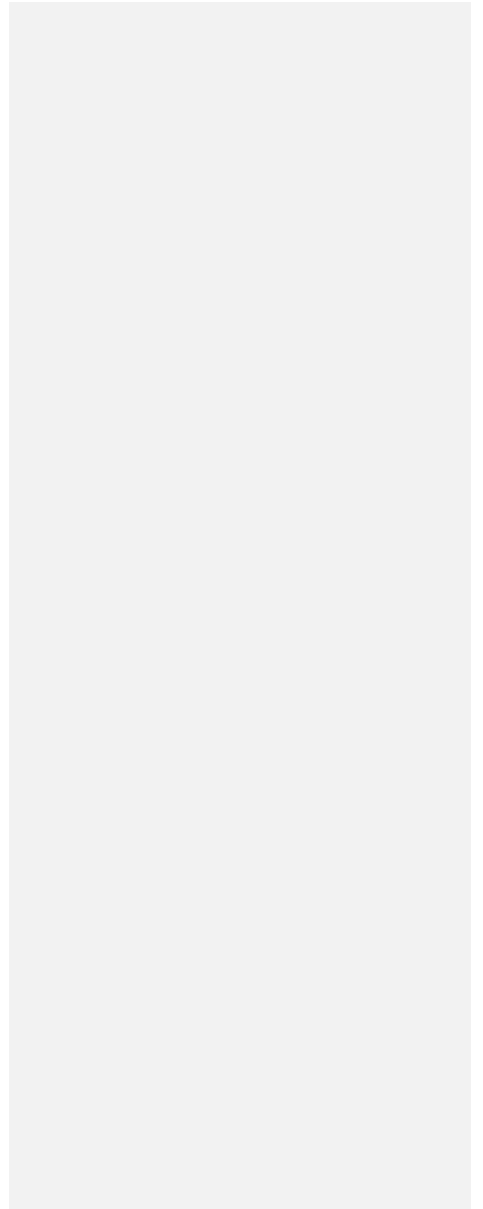
452

453
454

455
456
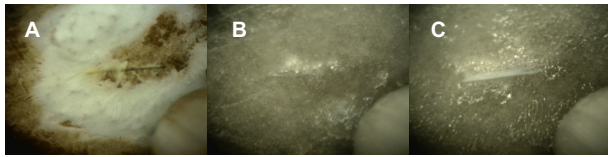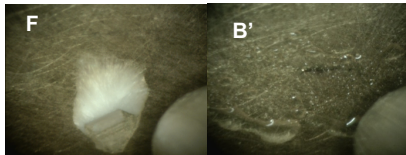
457 **Figure 5:** Optical microscopy pictures of the frozen samples. Each picture shows a 1 mm wide section of the sample holder with the
458 sample. The letters refer to the samples in Figs. 3 and 4: **A** Solid NaCl at 248 K and 44 % relative humidity. **B** Ice with brine at 88 %
459 RH and 259 K. Picture B' shows the deliquesced sample prior to freezing. **C** Sample below the eutectic temperature at 248 K to 249 K
460 in the presence of ice. **F** Sample in absence of ice at a relative humidity lower than 73 % and at 244 K. Pictures of samples D and E
461 were not taken. Picture B' shows the deliquesced sample prior to freezing.

462

463

464

Efflorescence at the interface

Now that we have identified halite, the hydrohalites, and ~~the~~ chloride in an aqueous solution by means of the NEXAFS spectra at the interfacial region, we discuss their observation in the phase diagram. Generally, we have observed solid sodium chloride as halite or hydrohalite at temperatures below in the temperature range of 24~~1~~0 K to 249 K and at 44 % to 79 % RH and brine in the temperature range of 248 K to 259 K and RH of 78 % - 88 %.

Interesti

ngly, the NEXAFS spectra have revealed the dominant presence of brine in one sample and of hydrohalite in other samples below the eutectic temperature. This clearly shows that not only the temperature and relative humidity, but also the trajectory to reach these settings (or the history of the sample) determines the phase. Therefore, we will detail the humidity and temperature history of each sample in the following. Also, we will compare our findings to the extensive literature work of observed phases in the presence and absence of ice. This discussion will be based on the ~~Figure 4A shows the~~ sodium chloride – water phase diagram in the temperature – relative humidity space (Figure 4) as initially constructed by Koop et al. (2000a). In this work, the relative humidity (RH) is referenced to the vapour pressure of (supercooled) water as parameterised by Marti and Mauersberger (1993). There are two sets of experiments, those where ice is ~~present~~present - and the sodium chloride is in equilibrium with ice (filled symbols) - and experiments in absence of ice (open symbols) that were done with a relative humidity less than the ice stability line in the phase diagram (dark blue line). ~~Generally, we have observed solid sodium chloride as halite or hydrohalite at temperatures below 240 K and at 44 % to 79 % RH and brine in the temperature range of 248 K to 259 K and RH of 78 % - 88 %.~~

Liquid below eutectic and nucleation

In a typical experiment, anhydrous salt was exposed to increased relative humidity at a fixed temperature of 259 K. ~~The relative humidity was increased by increasing the flux of water vapour~~

492 into the experimental cell. Once the relative humidity reached 72 %, the sample started to dissolve
493 by water up-take from the gas-phase and an aqueous solution was formed (brine). This phase
494 change was evident by the sample becoming shiny and then forming transparent spheres as
495 observed by an endoscope digital camera (Fig. 5B'). Then, the relative humidity was further
496 increased and/or temperature was lowered to cross the ice stability line until ice nucleation
497 occurred at a modest oversaturationsupersaturation of typically 90 % to 95 % relative humidity at
498 259 K. This relative humidity range corresponds to a supersaturation with respect to ice of 103 %
499 to 109 %. Ice nucleation was evident by a sharp pressure drop from the pressure dosed to the cell
500 to the water vapor pressure of ice at that temperature, for example 88 % relative humidity at 259 K.
501 In some experiments, temperature was lowered 1 K to 2 K as well to trigger ice nucleation. Please
502 note, that temperature was always well above the homogenous freezing temperature, which was
503 found at 210 K to 230 K at relative humidity of 60 % to 90 % (Koop et al., 2000a). Generally, in
504 the presence of ice, the partial pressure of water in the flow-through cell is given by the vapor
505 pressure of ice and is thus a sole function of temperature. If the water vapour pressure upstream of
506 the flow through cell exceeds this value, the ice on the sample holder is growing, if it is set below,
507 the ice sublimates. Based on the calibration of the dosing reservoir temperature and partial pressure
508 of water in the flow-through cell (in absence of ice), the incoming H_2O vapour flux was adjusted
509 such that the equilibrium pressure in the cell matched the vapour pressure of ice.
510
511 A NEXAFS spectrum was acquired at 259 K and 1.82 mbar on the ice stability line and taken as
512 reference for aqueous sodium chloride solution (Fig. 3B). When the temperature was lowered
513 while adapting the flux of water into the set-up to match the vapour pressure of ice at 248 K -
514 249 K, thus 3 K to 4 K below the eutectic temperature (Fig. 4B), the NEXAFS spectra revealed
515 that the chloride at the air-ice interface is in an environment identical to aqueous chloride (Fig.
516 3C). While cooling further and adjusting the vapor pressure to match that of ice at each
517 temperature, a sudden change in the sample appearance, becoming less transparent, was observed
518 by the digital endoscope, indicating efflorescence of the sample. A NEXAFS spectrum recorded
519 reveals that hydrohalite has precipitated from the brine at 2410.5 K and 74 % RH (Fig. 3D).

520 Krepelova et al. (2010a) has studied phase changes of sodium chloride at the interfacial region of

521 sodium chloride – water binary mixtures previously. They have probed the oxygen with XPS and

522 by partial electron yield NEXAFS spectroscopy and concluded that, in the presence of ice,

523 hydrohalite forms about 11 K below the eutectic (filled star in Fig. 4). Consistent with that, the

524 chloride has a local environment indistinguishable from that of the hydrohalite 11.4 K below the

525 eutectic temperature and in the presence of ice in the current study (Fig. 3D). Our results of

526 precipitation in the presence of ice surfaces agree with the crystallization temperature observed by

527 Koop et al. (2000a). We lack a direct comparison to the bulk, because the electron yield NEXAFS

528 spectroscopy used in our work is inherently surface sensitive. Cooling sodium chloride solutions of

529 varying concentration, Koop et al. (2000a) found precipitation of hydrohalite at 240 K in the

530 presence of ice for bulk samples. Because precipitation occurred at 20 K higher temperatures

531 compared to emulsion samples of the same concentration, the authors concluded that the presence

532 of surfaces enhance the crystallization rate. In that study, the hydrohalite was identified by the

533 melting temperatures of the ice-hydrohalite mixtures. Malley et al. (2018) observed crystallization

534 of sodium chloride solutions 1 K below the eutectic temperature in the presence of ice. The

535 hydrohalite was clearly identified using bulk sensitive Raman spectroscopy. This difference in

536 crystallization temperature may reflect the stochastic character of freezing, as already noted by

537 Koop et al. (2000a) when discussing the scatter in their data. The precise crystallization

538 temperature is also influenced by freezing rate, concentration, and the availability of surfaces

539 (Bartels-Rausch et al., 2014). It appears thus that the precise occurrence of crystallisation is

540 governed by stochastics both at the surface and as has been shown for in heterogeneous freezing of

541 the bulk samples (Alpert and Knopf, 2016) and by experimental settings. Because of the good

542 agreement between the precipitation temperatures observed in this study and in Koop et al.

543 (2000a), we believe that the deviation from Malley et al. (2018)'s results does not indicate

544 differences in the freezing behaviour at the surface vs. that in the bulk.

545

546 To investigate whether or notthe impact of the sample's history on the phase precipitated sodium

547 chloride is the stable form at the interface at temperatures close to the eutectic temperature, the

548 sample at 2410 K (green filled trianglediamond, Fig. 4B) was warmed towards the eutectic

549 temperature while staying in the ice stability domain. Acquiring a NEXAFS spectrum 3 K below

550 the eutectic temperature (Fig. 3E) that resembles that of hydrohalite, shows that the solid salt is

551 theliquid brine is not the thermodynamically stable form also at temperatures close to the eutectic.

552 We therefore interpret the existence of liquid during the previous cooling of the sample (Fig. 4B,

553 orange circle, Fig. 3C) at the interface as supercooled solution. The sample was kept at this

554 condition for 3 h. and showingThis shows that liquid can exist for extended times at the air-ice

555 interface below the eutectic temperature and that the temperature alone is not sufficient to predict

556 its presence. Rather the thermal history of the snow frozen matrix needs to be considered.

557

558 For samples that were cooled to temperatures that triggered efflorescence, the chlorine NEXAFS

559 spectra show that the hydrohalite is the dominating phase at the interface of frozen sodium chloride

560 – water binary mixtures. Cho et al. (2002) have shown that when frozen aqueous solutions were

561 warmed, a liquid fraction was observed below the eutectic temperatures. In their experiments, ice

562 was frozen in NMR tubes lowering the temperature to 228 K in 15 min. which is significantly

563 colder than the efflorescence temperatures observed here and by Koop et al. (2000a). After 10

564 minutes, the samples were warmed and NMR signals were recorded. Interestingly, Cho et al.

565 (2002) have observed the liquid fraction only in experiments where the sodium chloride

566 concentration in the initial aqueous solution was below 0.01 mol l^{-1}. If the initial aqueous solution

567 had a concentration of 0.5 mol l^{-1} no indication of liquid features below the eutectic were found.

568 Tasaki et al. (2010) has shown a similar concentration dependence for sodium bromide solutions

569 using X-ray absorption reporting solvated bromide in the bulk of the samples below the eutectic

570 temperature only for concentrations below 50 mmol l^{-1}.

571

572

573 We will now detail the concentration of brine in the study presented here to elaborate if differences

574 in concentration might explain the differences in the observed liquid content of sub-eutectic

575 samples. The experiments described here started the freezing process with an aqueous solution that

576 was formed in-situ and was kept in equilibrium with a vapour pressure of roughly 1.9 mbar. The
577 chloride concentration in such solutions is close to the concentration in a solution at 1.8 mbar and
578 at 259 K, where ice nucleation occurred and where the freezing point depression data give a
579 concentration of 3.5 mol l^{-1}. This concentration can be directly compared to the concentration in
580 the initial solutions of Cho et al. (2002), which ranged from below 0.01 mol l^{-1} to 0.5 mol l^{-1}. This
581 back-of-the-envelope calculation thus suggests that the concentration of the solutions from which
582 ice nucleated in the experiments reported here exceeded those described by Cho et al. (2002) for
583 which no liquid fraction was observed.
584
585 Next, we discuss how higher concentrations of initial solution might impact the location of brine in
586 the frozen matrix. The Now, the concentration of the initial solution from which ice precipitated,
587 determines the ice to brine ratio after ice formation. This is , because as the concentration of the
588 brine is a sole function of temperature, the volume of the brine relative to that of ice is given by the
589 water to sodium chloride ratio in the initial solution. The concentration of the brine in the presence
590 of ice is a sole function of temperature, and not of the initial concentration of the solution. One
591 might speculate that with large amounts of brine relative to ice, that is concentrations of initial
592 solutions from which ice nucleates > 0.5 mol l^{-1}, patches and inclusions are larger in size than for
593 more dilute solutions. The size of these patches or inclusions is of relevance, as surface forces
594 reduce the melting point only for inclusions in the nanometre range (Nye, 1991; Aristov et al.,
595 1997; Christenson, 2001; Bartels-Rausch et al., 2014). The absence of this so-called inverse Köhler
596 effect in larger particles patches or inclusions might explain the lack of liquid features both in the
597 results reported here at the interface of ice and in the high concentration samples of Cho et al.
598 (2002). Support for large patches at the interface when solutions are frozen comes from
599 microscopy a number of studies (Krausko et al., 2014; Tokumasu et al., 2016; Lieb-Lappen et al.,
600 2017; Malley et al., 2018). LLow temperature scanning electron microscopy work suggested the
601 ice surface of frozen 0.05 mol l^{-1} sodium chloride – water mixtures being covered by μm sized
602 brine features (Blackford, 2007; Blackford et al., 2007). Malley et al. (2018) used Raman
603 microscopy of sodium chloride solutions between 0.02 – 0.6 mol l^{-1} initial concentration to identify

604 micrometre-sized, partially connected patches of liquid covering 11 % to 85 % of the ice surface at
605 temperatures above the eutectic. Despite the impact of freezing temperature and rate -- that differs
606 among the individual studies -- on the distribution of impurities (Bartels-Rausch et al., 2014;
607 Hullar and Anastasio, 2016), these results clearly show the tendency of μm sized features
608 dominating at the air-ice interface. In the dominant presence of nano-inclusions, we would also
609 expect the deliquescence to occur at a lower temperature. This was not observed in our
610 experiments, suggesting the absence of nano-inclusions in the experiments presented here in the
611 interfacial region. Please note, that the NEXAFS spectroscopy presented here probes an area at the
612 interface of the sample with a diameter of about 500 μm. As the spectroscopy is selective to
613 chlorine, we have no information about the fraction of ice in the probed part of the sample.
614
615 The previous argumentation is based on We have recently reported chloride forming solvation
616 shells in the interfacial region of ice upon adsorption of HCl at 253 K (Kong et al., 2017). The
617 surface concentration as derived from XPS suggested that it was done in the stability domain of
618 ice, i.e., the concentration of HCl was too low to melt the ice. Oxygen K-edge NEXAFS spectra
619 showed that a substantial fraction of the water molecules at the air-ice interface is arranged in a
620 hydrogen-bonding structure like that of liquid water. tThe features in the NEXAFS spectrum of
621 sodium chloride – ice mixtures (Fig. 3E) at 249 Kshown in Fig. 3 D and E are being
622 indistinguishable dominated from thoseby the hydrohalite as seen in the NEXAFS spectrum of
623 hydrohaliteshown in Fig. 3F. In particular the spectrum in Fig. 3E, acquired 3 K below the eutectic
624 temperature, shows a shoulder starting at 2823 eV. Such a feature is absent in the spectrum of the
625 hydrohalite (Fig. 3 F), but the spectrum of brine (Fig. 3 B) shows an increase in absorption starting
626 at this X-ray energy. This feature might thus indicate small amounts of brine and we can thus not
627 exclude the presence of brine in the samples where the hydrohalite dominates the NEXAFS.
628 Taken the spectra quality and the small difference in the shape of the liquid and of the hydrohalite
629 spectrum, it is beyond the scope of this work to elaborate whether the NEXAFS spectrum in Fig.
630 3E might be understood by deconvoluting it in its hydrohalite and brine components and by this
631 reveal a fraction of the chloride being embedded in a brine-like hydrogen bonding network. Two

632 reasons might explain the presence of liquid-like feature in the NEXAFS spectra at sub-eutectic

633 temperatures. First, one might expect a certain distribution in the size of micropockets and a

634 fraction of the pockets might thus be small enough to stabilize liquid at these temperatures.

635 Secondly, some of the chloride might form solvation shells with water molecules from the ice

636 matrix as proposed for trace gases adsorbed to ice (Krepelova et al., 2010b; Krepelova et al., 2013;

637 Bartels-Rausch et al., 2017). In particular, ~~Krepelova et al. (2010a)'s oxygen K-edge spectra of~~

638 ~~sodium chloride -- ice did not reveal water molecules being coordinated like in the liquid. w~~We

639 have recently reported chloride forming solvation shells in the interfacial region of ice upon

640 adsorption of HCl at 253 K (Kong et al., 2017). The surface concentration as derived from XPS

641 suggested that it was done in the stability domain of ice, i.e., the concentration of HCl was too low

642 to melt the ice. Oxygen K-edge NEXAFS spectra showed that a substantial fraction of the water

643 molecules at the air-ice interface is arranged in a hydrogen-bonding structure like that of liquid

644 water. We like to note, that Krepelova et al. (2010a)'s oxygen K-edge spectra of sodium chloride --

645 ice did not reveal water molecules being coordinated like in the liquid. Taken together ~~it seems~~

646 ~~likely that the chloride at the hydrohalite – air interface does not engage in forming solvation shells~~

647 ~~similar to those in aqueous solutions and that~~ the signal from the hydrohalite by far exceeds the

648 signal from a chloride ~~that~~ in brine or in an liquid-like environment at the molecular level~~might~~

649 ~~migrate to the ice surfaces~~ in intensity.

650 **Nucleation in absence of ice**

651 Hydrohalite can also precipitate in absence of ice by evaporating water from a solution at

652 temperatures below 273 K (Craig et al., 1975; Yang et al., 2017). Such a trajectory, that is the

653 temperature and water vapor pressure the sample experienced, is shown in Fig. 4C (green solid

654 line). In this set of experiments, water was evaporated by decreasing the relative humidity to about

655 70 % at 252 K from a brine sample in absence of ice, followed by lowering the temperature to

656 247 K at constant partial pressure of water (so that the relative humidity increased to about 80 %).

657 When the ice stability line in the phase diagram was crossed, ice nucleation was not observed as

658 the oversaturation was not sufficient to trigger ice nucleation. This procedure was repeated to

659 further lower the temperature to 244 K at 59 % relative humidity. Then, ~~Two NEXAFS spectra~~

660 ~~were recorded (Fig. 4, green diamonds), both of which were identified as hydrohalite (Fig. 3F).~~

661 tThe first ~~one~~ NEXAFS was recorded at 244 K and 59 % RH (Fig. 4, green diamond), where in

662 absence of ice nucleation was visually observed. ~~-~~The location in the phase diagram is in

663 agreement with Wagner et al. (2012)'s observation of salt deposits in aerosol droplets in an aerosol

664 chamber (AIDA) in absence of ice. The second NEXAFS spectra ~~resembling that of the~~

665 ~~hydrohalite and in absence of ice~~ was recorded at a slightly higher relative humidity of ~~72~~ 73 %

666 (Fig. 4, green diamond). Both NEXAFS spectra (Fig. 4, green diamonds) were identified as

667 hydrohalite (Fig. 3F).

668

669 The sample at 44 % RH (Fig. ~~4C, blue line~~3A) has been exposed to 0 % RH prior to acquiring the

670 NEXAFS spectrum (Fig. 4C, blue square and blue line), which removes the crystal water (Light et

671 al., 2009; Wise et al., 2012). This NEXAFS spectrum recorded at 248 K and 44 % RH shows that

672 no deliquescence occurred and thus serves as reference for a halite spectrum (Fig. ~~1A~~3A). We note

673 that we misinterpreted this spectrum as that of hydrohalite in our previous technical paper

674 introducing the NAPP end station (Orlando et al., 2016).

675

676 The halite spectrum (Fig. 3A, Fig. 4C blue square) was recorded at 44 % RH, a humidity where

677 water readily adsorbs on surfaces (Bluhm, 2010), and the presence of water at the sodium chloride

678 - air interface at elevated RH has been demonstrated previously (Ewing, 2005; Wise et al., 2008).

679 A further reason for the presence of water at lower RH than the deliquescence might be sodium

680 chloride's high solubility. Kong et al. (2020) has recently suggested that sodium ions from sodium

681 acetate are dissolved in adsorbed water prior to deliquescence. Indications for solvation of halide

682 ions on single crystals below deliquescence relative humidity were also reported previously (Luna

683 et al., 1998). An analogue investigation was beyond the scope of this work. The fact that we find

684 no indication for a dominant liquid feature in the upper 6 nm of the sodium chloride – air interface

685 based on the chlorine X-ray absorption spectrum might be due to probing deeper into the

686 interfacial region in this work as compared to Kong et al. (2020).

NaCl or NaCl·2H$_2$O

We have shown that in the presence of ice, hydrohalite precipitates; halite was not observed in this study except when crystal water was removed in vacuum. This ~~is in agreement~~agrees with Koop et al. (2000a) who found precipitation of hydrohalite in the presence of ice and suggested that heterogenous nucleation at ice surfaces favours nucleation of hydrohalite. Studies with liquid droplets in absence of ice found both halite and hydrohalite precipitating in the thermodynamic stability domain of the hydrohalite (Wagner et al., 2011; Wise et al., 2012; Peckhaus et al., 2016). The transition between crystallization of halite and hydrohalite at between 253 K to 241 K was explained based on nucleation theory and the deviating trend of nucleation rate of both species with temperature (Peckhaus et al., 2016). That hydrohalite crystallizes in absence of ice in our study shows that also gold surfaces, of the sample holder, serve as good nucleation support for hydrohalite. It appears that any specific properties of the ice surface, as compared to gold, are of minor importance. In agreement, Wagner et al. (2015) showed efficient nucleation of hydrohalite in droplets containing solid oxalic acid and halite precipitated in absence of oxalic acid at the same temperature and relative humidity.

1 Summary and Atmospheric Implication

The upper few nanometre (mean electron escape depth of 6 nm) of the interfacial region of a sodium chloride – ice binary system was investigated in this study at various positions in the phase diagram. The sample was always in equilibrium with gas-phase water which makes cooling conditions ~~and concentrations of the brine~~ identical and concentration of brine similar to that of aerosol particles embedded in snow or in the troposphere. ~~The~~The inherent sensitivity to the interfacial region comes from using partial Auger-Meitner electron yield NEXAFS and the limited pathlength of electrons travelling in matter. With a mean electron escape depth of 6 nm ~~probing depth of a few nanometre~~, the interfacial region is probed spanning from the upper molecular layers somewhat into the bulk (Ammann et al., 2018). In this work, we describe the NEXAFS spectrum of hydrohalite for the first time.

713

714 The results emphasise that the nucleation of hydrohalite is a function of both the temperature and

715 the relative humidity. While we show that the nucleation of hydrohalite at the interface is favoured

716 by surfaces, we find supercooled solution of sodium chloride in the interfacial region of ice. The

717 supercooled solutions have been observed to be metastable for hours in these experiments. This has

718 direct implications for heterogeneous chemistry in cold parts of Earth's environment. Multiphase

719 reactions may proceed at accelerated rates in these highly concentrated brines at temperatures ~10

720 degrees below the eutectic compared to reactions on solid hydrohalite. This temperature range of

721 ~241 K is frequently observed in polar coastal sites during spring and in the free troposphere. In

722 this respect, there is no difference in the interfacial region to liquid embedded in the bulk of snow

723 and ice samples. This implies that when chemical reactivity of ice and snow is discussed,

724 knowledge of its thermal history is essential. From temperature and relative humidity alone,

725 nucleation or efflorescence cannot be predicted at the interface as in the bulk. We suggest that

726 further studies focus on samples with more complex chemical composition to enhance our

727 knowledge of environmental multiphase chemistry. For example, organic compounds are a

728 common constituent of sea-salt aerosol (O'Dowd et al., 2004) Kirpes et al. (2019) and Edebeli et al.

729 (2019) have shown how the presence of organics impacts the microphysics and thus reactivity of

730 salt particles towards ozone(Edebeli et al., 2019). Further, Chakraborty and Kahan (2020) have

731 shown a depression in hydrohalite precipitation temperature in humic acid – sodium chloride

732 mixtures.

733

734 We suggest that the brine observed by Cho et al. (2002) is a consequence of the presence of very

735 small micro-pockets holding the brine. Because these pockets only tend to be small enough to

736 establish a significant depression in freezing point when solutions with are only observed at low

737 concentration of the solution before freezing of iceare freezing, but and because aerosol at typical

738 relative humidity that prevail in cold parts of the atmosphere are highly concentrated;, we suggest

739 that such micronano-pockets in the interfacial region small enough to establish a significant

740 depression in freezing point at the air-ice interface are of small relevance to the environment.

741

742

743

744 The appearance of hydrohalite at air-ice interfaces might also be of interest to sea ice research,

745 because precipitation of hydrohalite increases the albedo of sea ice. During the Snowball Earth

746 period, 700 million years before present, climatic conditions may have favoured the existence of

747 hydrohalite with its climatic feedback (Light et al., 2009). For modern Earth, precipitation of brine

748 constituents in sea ice is relevant for ion mobility and might result in ion fractionation during wash

749 out events (Maus et al., 2008; Obbard et al., 2009; Maus et al., 2011) and possibly brine migration

750 upwards through the snow (Dominé et al., 2004).

751

752 Precipitation of sodium chloride in sea spray aerosol in the troposphere, not embedded in snow or

753 sea ice, is further of ongoing interest. Again, the Arctic coastal areas are of high relevance here,

754 because temperature and relative humidity frequently favour precipitation of hydrohalite. Other

755 studies have focus on the temperature range of 230 K to 260 K at a relative humidity of 30 % to

756 70 % (see Fig. 4 and references therein) to explore the precipitation in the dryer free troposphere.

757 The Research focusedfocus is placed on whether anhydrous sodium chloride (halite) or hydrohalite

758 precipitates. In regions of the phase diagram, where the hydrohalite is the thermodynamic stable

759 form, precipitation of the halite was observed with impacts on stability of the solid phase upon

760 warming and or humidification, since the deliquesce relative humidity of the two compounds

761 differs by 6 percentage points (Wagner et al., 2012; Wise et al., 2012; Peckhaus et al., 2016).

Data Availability

Bartels-Rausch, Thorsten (2020). Data set on interfacial supercooling and the precipitation of

hydrohalite in frozen NaCl solutions by X-ray absorption spectroscopy. EnviDat.

doi:10.16904/envidat.164.

Acknowledgement

Funding by the Swiss National Science Foundation (SNSF) under Grant No. 149629 is

acknowledged. We thank Mario Birrer (PSI) for his technical assistance. TB-R thanks Peter Alpert

for stimulating discussion in our office. We thank the SLS team and Phoenix beamline team for

their assistance and for providing a stable and brilliant beam.

Author Contribution

TB-R designed and planned the study, analysed the data, and wrote the manuscript. FO, LA, MA,

TH planned and optimised beamline and electron analyser settings. XK, AW, LA, and TBR

performed the experiments. All authors approved the submitted version of the manuscript.

References

Abbatt, J. P. D., Thomas, J. L., Abrahamsson, K., Boxe, C. S., Granfors, A., Jones, A. E., King, M. D., Saiz-Lopez, A.,
Shepson, P. B., Sodeau, J. R., Toohey, D. W., Toubin, C., von Glasow, R., Wren, S. N., and Yang, X.: Halogen activation
via interactions with environmental ice and snow in the polar lower troposphere and other regions, Atmos. Chem. Phys.,
12, 6237-6271, 10.5194/acp-12-6237-2012, 2012.

Alpert, P. A., and Knopf, D. A.: Analysis of isothermal and cooling-rate-dependent immersion freezing by a unifying
stochastic ice nucleation model, Atmos. Chem. Phys., 16, 2083-2107, 10.5194/acp-16-2083-2016, 2016.

Ammann, M., Artiglia, L., and Bartels-Rausch, T.: X-ray excited electron spectroscopy to study gas–liquid interfaces of
atmospheric relevance, in: Physical chemistry of gas-liquid interfaces, Elsevier, 135-166, 2018.

Antalek, M., Pace, E., Hedman, B., Hodgson, K. O., Chillemi, G., Benfatto, M., Sarangi, R., and Frank, P.: Solvation
structure of the halides from x-ray absorption spectroscopy, J. Chem. Phys., 145, 044318, 10.1063/1.4959589, 2016.

787   Aristov, Y. I., Di Marco, G., Tokarev, M. M., and Parmon, V. N.: Selective water sorbents for multiple applications, 3.
788   CaCl2 solution confined in micro- and mesoporous silica gels: Pore size effect on the "solidification-melting" diagram,
789   React. Kinet. Catal. Lett., 61, 147-154, 10.1007/BF02477527, 1997.

790   Artiglia, L., Edebeli, J., Orlando, F., Chen, S., Lee, M.-T., Corral Arroyo, P., Gilgen, A., Bartels-Rausch, T., Kleibert,
791   A., Vazdar, M., Carignano, M. A., Francisco, J. S., Shepson, P. B., Gladich, I., and Ammann, M.: A surface-stabilized
792   ozonide triggers bromide oxidation at the aqueous solution-vapour interface, Nat. Commun., 8, 700, 10.1038/s41467-
793   017-00823-x, 2017.

794   Bartels-Rausch, T., Jacobi, H.-W., Kahan, T. F., Thomas, J. L., Thomson, E. S., Abbatt, J. P. D., Ammann, M.,
795   Blackford, J. R., Bluhm, H., Boxe, C. S., Dominé, F., Frey, M. M., Gladich, I., Guzman, M. I., Heger, D., Huthwelker,
796   T., Klan, P., Kuhs, W. F., Kuo, M. H., Maus, S., Moussa, S. G., McNeill, V. F., Newberg, J. T., Pettersson, J. B. C.,
797   Roeselova, M., and Sodeau, J. R.: A review of air–ice chemical and physical interactions (AICI): Liquids, quasi-liquids,
798   and solids in snow, Atmos. Chem. Phys., 14, 1587-1633, 10.5194/acp-14-1587-2014, 2014.

799   Bartels-Rausch, T., Orlando, F., Kong, X., Artiglia, L., and Ammann, M.: Experimental evidence for the formation of
800   solvation shells by soluble species at a nonuniform air-ice interface, ACS Earth Space Chem., 1, 572-579,
801   10.1021/acsearthspacechem.7b00077, 2017.

802   Blackford, J. R.: Sintering and microstructure of ice: A review, J. Phys. D: Appl. Phys., 40, R355-R385, 10.1088/0022-
803   3727/40/21/R02, 2007.

804   Blackford, J. R., Jeffree, C. E., Noake, D. F. J., and Marmo, B. A.: Microstructural evolution in sintered ice particles
805   containing NaCl observed by low-temperature scanning electron microscope, Proc. Inst. Mech. Eng, 221, 151-156,
806   10.1243/14644207JMDA134, 2007.

807   Bluhm, H., Ogletree, D. F., Fadley, C. S., Hussain, Z., and Salmeron, N.: The premelting of ice studied with
808   photoelectron spectroscopy, J. Phys.: Condens. Matter, 14, L227-L233, 10.1088/0953-8984/14/8/108, 2002.

809   Bluhm, H.: Photoelectron spectroscopy of surfaces under humid conditions, Journal of Electron Spectroscopy and
810   Related Phenomena, 177, 71-84, 10.1016/j.elspec.2009.08.006, 2010.

811   Chakraborty, S., and Kahan, T. F.: Physical characterization of frozen aqueous solutions containing sodium chloride and
812   humic   acid   at   environmentally   relevant   temperatures,   ACS   Earth   Space   Chem.,   4,   305-310,
813   10.1021/acsearthspacechem.9b00319, 2020.

814   Cho, H., Shepson, P. B., Barrie, L. A., Cowin, J. P., and Zaveri, R.: NMR investigation of the quasi-brine layer in
815   ice/brine mixtures, J. Phys. Chem. B, 106, 11226-11232, 10.1021/jp020449+, 2002.

816   Christenson, H. K.: Confinement effects on freezing and melting, J. Phys.: Condens. Matter, 13, R95-R133,
817   10.1088/0953-8984/13/11/201, 2001.

818   Cleff, B., and Mehlhorn, W.: Das KLL- Auger-Spektrum von Chlor, Z. Phys. A: Hadrons Nucl., 219, 311-324,
819   10.1007/BF01395528, 1969.

820 Craig, J. R., Light, J. F., Parker, B. C., and Mudrey, M. G.: Identification of hydrohalite, Antarctic Journal of the United
821 States, 10, 178-179, 1975.

822 Custard, K. D., Raso, A. R. W., Shepson, P. B., Staebler, R. M., and Pratt, K. A.: Production and release of molecular
823 bromine and chlorine from the arctic coastal snowpack, ACS Earth Space Chem., 1, 142-151,
824 10.1021/acsearthspacechem.7b00014, 2017.

825 Dominé, F., and Shepson, P. B.: Air-snow interactions and atmospheric chemistry, Science, 297, 1506-1510,
826 10.1126/science.1074610, 2002.

827 Dominé, F., Sparapani, R., Ianniello, A., and Beine, H. J.: The origin of sea salt in snow on arctic sea ice and in coastal
828 regions, Atmos. Chem. Phys., 4, 2259-2271, 2004.

829 Edebeli, J., Ammann, M., and Bartels-Rausch, T.: Microphysics of the aqueous bulk counters the water activity driven
830 rate acceleration of bromide oxidation by ozone from 289–245 K, Environ Sci Process Impacts, 21, 63-73,
831 10.1039/c8em00417j, 2019.

832 Evans, K. A., Mavrogenes, J. A., O'Neill, H. S., Keller, N. S., and Jang, L. Y.: A preliminary investigation of chlorine
833 XANES in silicate glasses, Geochem. Geophys. Geosyst., 9, 10.1029/2008gc002157, 2008.

834 Ewing, G. E.: H2O on NaCl: From single molecule, to clusters, to monolayer, to thin film, to deliquescence, in, Chapter
835 12, Springer-Verlag, Berlin/Heidelberg, 1-25, 2005.

836 Finlayson-Pitts, B. J.: The tropospheric chemistry of sea salt: A molecular-level view of the chemistry of NaCl and
837 NaBr, Chem. Rev., 103, 4801-4822, 10.1021/cr020653t, 2003.

838 Finlayson-Pitts, B. J.: Halogens in the troposphere, Anal. Chem., 82, 770-776, 10.1021/ac901478p, 2010.

839 Fujimori, T., Takaoka, M., and Morisawa, S.: Chlorinated aromatic compounds in a thermal process promoted by
840 oxychlorination of ferric chloride, Environ. Sci. Technol., 44, 1974-1979, 10.1021/es903337d, 2010.

841 Gladich, I., Chen, S., Vazdar, M., Boucly, A., Yang, H., Ammann, M., and Artiglia, L.: Surface propensity of aqueous
842 atmospheric bromine at the liquid-gas interface, J Phys Chem Lett, 11, 3422-3429, 10.1021/acs.jpclett.0c00633, 2020.

843 Grannas, A. M., Bausch, A. R., and Mahanna, K. M.: Enhanced aqueous photochemical reaction rates after freezing, J.
844 Phys. Chem. A, 111, 11043-11049, 10.1021/jp073802q, 2007.

845 Halfacre, J. W., Shepson, P. B., and Pratt, K. A.: Ph-dependent production of molecular chlorine, bromine, and iodine
846 from frozen saline surfaces, Atmos. Chem. Phys., 19, 4917-4931, 10.5194/acp-19-4917-2019, 2019.

847 Harada, M., Tasaki, Y., Tasaki, Y., Qu, H., and Okada, T.: Hydration of ions and salt crystallization in liquid phase
848 coexistent with ice at temperature below eutectic point, RSC Advances, 2, 461-466, 10.1039/c1ra00801c, 2011.

849 Huggins, F. E., and Huffman, G. P.: Chlorine in coal - an XAFS spectroscopic investigation, Fuel, 74, 556-569,
850 10.1016/0016-2361(95)98359-m, 1995.

851 Hullar, T., and Anastasio, C.: Direct visualization of solute locations in laboratory ice samples, Cryosphere, 10, 2057-
852 2068, 10.5194/tc-10-2057-2016, 2016.

853 Kahan, T. F., Wren, S. N., and Donaldson, D. J.: A pinch of salt is all it takes: Chemistry at the frozen water surface,
854 Acc. Chem. Res. , 47, 1587-1594, 10.1021/ar5000715, 2014.

855 Kirpes, R. M., Bonanno, D., May, N. W., Fraund, M., Barget, A. J., Moffet, R. C., Ault, A. P., and Pratt, K. A.:
856 Wintertime arctic sea spray aerosol composition controlled by sea ice lead microbiology, ACS Cent Sci, 5, 1760-1767,
857 10.1021/acscentsci.9b00541, 2019.

858 Klewe, B., Pedersen, B., and Iucr: The crystal structure of sodium chloride dihydrate, Acta Crystallogr., Sect. B, 30,
859 2363-2371, 10.1107/S0567740874007138, 1974.

860 Knipping, E. M., Lakin, M. J., Foster, K. L., Jungwirth, P., Tobias, D. J., Gerber, R. B., Dabdub, D., and Finlayson-Pitts,
861 B. J.: Experiments and simulations of ion-enhanced interfacial chemistry on aqueous NaCl aerosols, Science, 288, 301-
862 306, 10.1126/science.288.5464.301, 2000.

863 Kong, X., Waldner, A., Orlando, F., Artiglia, L., Huthwelker, T., Ammann, M., and Bartels-Rausch, T.: Coexistence of
864 physisorbed and solvated HCl at warm ice surfaces, J. Phys. Chem. Lett., 8, 4757-4762, 10.1021/acs.jpclett.7b01573,
865 2017.

866 Kong, X., Castarède, D., Boucly, A., Artiglia, L., Ammann, M., Bartels-Rausch, T., Thomson, E. S., and Pettersson, J.
867 B. C.: Reversibly physisorbed and chemisorbed water on carboxylic salt surfaces under atmospheric conditions, J. Phys.
868 Chem. C, 124, 5263-5269, 10.1021/acs.jpcc.0c00319, 2020.

869 Koop, T., Kapilashrami, A., Molina, L. T., and Molina, M. J.: Phase transitions of sea-salt/water mixtures at low
870 temperatures: Implications for ozone chemistry in the polar marine boundary layer, J. Geophys. Res., 105, 26393-26402,
871 10.1029/2000JD900413, 2000a.

872 Koop, T., Luo, B. P., Tsias, A., and Peter, T.: Water activity as the determinant for homogeneous ice nucleation in
873 aqueous solutions, Nature, 406, 611-614, 10.1038/35020537, 2000b.

874 Krausko, J., Runštuk, J., Neděla, V., Klan, P., and Heger, D.: Observation of a brine layer on an ice surface with an
875 environmental scanning electron microscope at higher pressures and temperatures, Langmuir, 30, 5441-5447,
876 10.1021/la500334e, 2014.

877 Krepelova, A., Huthwelker, T., Bluhm, H., and Ammann, M.: Surface chemical properties of eutectic and frozen NaCl
878 solutions probed by XPS and NEXAFS, Chem. Phys. Chem., 11, 3859-3866, 10.1002/cphc.201000461, 2010a.

879 Krepelova, A., Newberg, J. T., Huthwelker, T., Bluhm, H., and Ammann, M.: The nature of nitrate at the ice surface
880 studied by XPS and NEXAFS, Phys. Chem. Chem. Phys., 12, 8870-8880, 10.1039/c0cp00359j, 2010b.

881 Krepelova, A., Bartels-Rausch, T., Brown, M. A., Bluhm, H., and Ammann, M.: Adsorption of acetic acid on ice studied
882 by ambient-pressure XPS and partial-electron-yield NEXAFS spectroscopy at 230–240 K, J. Phys. Chem. A, 117, 401-
883 409, 10.1021/jp3102332, 2013.

884 Laskin, A., Wang, H., Robertson, W. H., Cowin, J. P., Ezell, M. J., and Finlayson-Pitts, B. J.: A new approach to
885 determining gas-particle reaction probabilities and application to the heterogeneous reaction of deliquesced sodium
886 chloride particles with gas-phase hydroxyl radicals, J. Phys. Chem. A, 110, 10619-10627, 10.1021/jp063263+, 2006.

887 Lieb-Lappen, R. M., Golden, E. J., and Obbard, R. W.: Metrics for interpreting the microstructure of sea ice using X-
888 ray micro-computed tomography, Cold Reg. Sci. Technol., 138, 24-35, 10.1016/j.coldregions.2017.03.001, 2017.

889 Light, B., Brandt, R. E., and Warren, S. G.: Hydrohalite in cold sea ice: Laboratory observations of single crystals,
890 surface accumulations, and migration rates under a temperature gradient, with application to "snowball earth", J.
891 Geophys. Res., 114, C07018, 10.1029/2008JC005211, 2009.

892 Lopez-Hilfiker, F. D., and Thornton, J. A.: Temperature dependent halogen activation by
893 n₂o₅ reactions on halide-doped ice surfaces, Atmos. Chem. Phys., 12,
894 5237-5247, 10.5194/acp-12-5237-2012, 2012.

895 Luna, M., Rieutord, F., Melman, N. A., Dai, Q., and Salmeron, M.: Adsorption of water on alkali halide surfaces studied
896 by scanning polarization force microscopy, J. Phys. Chem. A, 102, 6793-6800, 10.1021/jp9820875, 1998.

897 Malley, P. P. A., Chakraborty, S., and Kahan, T. F.: Physical characterization of frozen saltwater solutions using Raman
898 microscopy, ACS Earth Space Chem., 2, 702-710, 10.1021/acsearthspacechem.8b00045, 2018.

899 Marti, J., and Mauersberger, K.: A survey and new measurements of ice vapor pressure at temperatures between 170 and
900 250 K, Geophys. Res. Lett., 20, 363-366, 10.1029/93GL00105, 1993.

901 Maus, S., Huthwelker, T., Enzmann, F., Miedaner, M. M., Stampanoni, M., Marone, F., Hutterli, M. A., Hintermüller,
902 C., Hintermüller, C., and Kersten, M.: Synchrotron-based X-ray micro-tomography: Insights into sea ice microstructure,
903 Sixth Workshop on Baltic Sea Ice Climate, Lammi Biological Station, Finland, Aug 25, 2008.

904 Maus, S., Huthwelker, T., Schwikowski, M., and Enzmann, F.: Ion fractionation in young sea ice from Kongsfjorden,
905 svalbard, Annals of Glaciology, 52, 301-310, Doi 10.3189/172756411795931804, 2011.

906 Murphy, D. M., Froyd, K. D., Bian, H., Brock, C. A., Dibb, J. E., DiGangi, J. P., Diskin, G., Dollner, M., Kupc, A.,
907 Scheuer, E. M., Schill, G. P., Weinzierl, B., Williamson, C. J., and Yu, P.: The distribution of sea-salt aerosol in the
908 global troposphere, Atmos. Chem. Phys., 19, 4093-4104, 10.5194/acp-19-4093-2019, 2019.

909 Newberg, J. T., and Bluhm, H.: Adsorption of 2-propanol on ice probed by ambient pressure X-ray photoelectron
910 spectroscopy, Phys. Chem. Chem. Phys., 17, 23554-23558, 10.1039/C5CP03821A, 2015.

911 Nilsson, A., Nordlund, D., Waluyo, I., Huang, N., Ogasawara, H., Kaya, S., Bergmann, U., Näslund, L. A., Öström, H.,
912 Wernet, P., Andersson, K. J., Schiros, T., and Pettersson, L. G. M.: X-ray absorption spectroscopy and X-ray Raman
913 scattering of water and ice; an experimental view, Journal of Electron Spectroscopy and Related Phenomena, 177, 99-
914 129, 10.1016/j.elspec.2010.02.005, 2010.

915 Nye, J. F.: Thermal behaviour of glacier and laboratory ice, J. Glaciol., 37, 401-413, 10.3189/S0022143000005839,
916 1991.

917 O'Dowd, C. D., Facchini, M. C., Cavalli, F., Ceburnis, D., Mircea, M., Decesari, S., Fuzzi, S., Yoon, Y. J., and Putaud,
918 J.-P.: Biogenically driven organic contribution to marine aerosol, Nature, 431, 676-680, 10.1038/nature02959, 2004.

919 Obbard, R. W., Troderman, G., and Baker, I.: Imaging brine and air inclusions in sea ice using micro-X-ray computed
920 tomography, J. Glaciol., 55, 1113-1115, Doi 10.3189/002214309790794814, 2009.

Oldridge, N. W., and Abbatt, J. P. D.: Formation of gas-phase bromine from interaction of ozone with frozen and liquid NaCl/NaBr solutions: Quantitative separation of surficial chemistry from bulk-phase reaction, J. Phys. Chem. A, 115, 2590-2598, 10.1021/jp200074u, 2011.

Orlando, F., Waldner, A., Bartels-Rausch, T., Birrer, M., Kato, S., Lee, M.-T., Proff, C., Huthwelker, T., Kleibert, A., van Bokhoven, J. A., and Ammann, M.: The environmental photochemistry of oxide surfaces and the nature of frozen salt solutions: A new in situ XPS approach, Top. Catal., 59, 591-604, 10.1007/s11244-015-0515-5, 2016.

Osthoff, H. D., Roberts, J. M., Ravishankara, A. R., Williams, E. J., Lerner, B. M., Sommariva, R., Bates, T. S., Coffman, D., Quinn, P. K., Dibb, J. E., Stark, H., Burkholder, J. B., Talukdar, R. K., Meagher, J., Fehsenfeld, F. C., and Brown, S. S.: High levels of nitryl chloride in the polluted subtropical marine boundary layer, Nat. Geosi., 1, 324-328, 10.1038/ngeo177, 2008.

Peckhaus, A., Kiselev, A., Wagner, R., Duft, D., and Leisner, T.: Temperature-dependent formation of NaCl dihydrate in levitated NaCl and sea salt aerosol particles, J. Chem. Phys., 145, 244503, 10.1063/1.4972589, 2016.

Petrich, C., and Eicken, H.: Growth, structure and properties of sea ice, Sea Ice, 23-77, doi:10.1002/9781444317145.ch2 10.1002/9781444317145.ch2, 2009.

Rumble, J.: CRC handbook of chemistry and physics, 100th edition, in, CRC Press/Taylor & Francis, Boca Raton, FL., 2019.

Saiz-Lopez, A., and von Glasow, R.: Reactive halogen chemistry in the troposphere, Chem. Soc. Rev., 41, 6448-6472, 10.1039/C2CS35208G, 2012.

Simpson, W. R., von Glasow, R., Riedel, K., Anderson, P., Ariya, P., Bottenheim, J., Burrows, J., Carpenter, L. J., Friess, U., Goodsite, M. E., Heard, D., Hutterli, M., Jacobi, H. W., Kaleschke, L., Neff, B., Plane, J., Platt, U., Richter, A., Roscoe, H., Sander, R., Shepson, P., Sodeau, J., Steffen, A., Wagner, T., and Wolff, E.: Halogens and their role in polar boundary-layer ozone depletion, Atmos. Chem. Phys., 7, 4375-4418, 10.5194/acp-7-4375-2007, 2007.

Simpson, W. R., Brown, S. S., Saiz-Lopez, A., Thornton, J. A., and von Glasow, R.: Tropospheric halogen chemistry: Sources, cycling, and impacts, Chem. Rev., 115, 4035-4062, 10.1021/cr5006638, 2015.

Sjostedt, S. J., and Abbatt, J. P. D.: Release of gas-phase halogens from sodium halide substrates: Heterogeneous oxidation of frozen solutions and desiccated salts by hydroxyl radicals, Environ. Res. Lett., 3, 045007, 10.1088/1748-9326/3/4/045007, 2008.

Tanuma, S., Powell, C. J., and Penn, D. R.: Calculations of electron inelastic mean free paths: 3. Data for 15 inorganic-compounds over the 50-2000 eV range, Surf. Interface Anal., 17, 927-939, 10.1002/sia.740171305, 1991.

Tasaki, Y., Harada, M., and Okada, T.: Eutectic transition of local structure for bromide ion in bulk and on surface of doped ice, J. Phys. Chem. C, 114, 12573-12579, 10.1021/jp102246f, 2010.

Thomas, J. L., Stutz, J., Frey, M. M., Bartels-Rausch, T., Altieri, K., Baladima, F., Browse, J., Dall'Osto, M., Marelle, L., Mouginot, J., Jennifer, G. M., Nomura, D., Pratt, K. A., Willis, M. D., Zieger, P., Abbatt, J., Douglas, T. A., Facchini, M. C., France, J., Jones, A. E., Kim, K., Matrai, P. A., McNeill, V. F., Saiz-Lopez, A., Shepson, P., Steiner, N., Law, K.

955 S., Arnold, S. R., Delille, B., Schmale, J., Sonke, J. E., Dommergue, A., Voisin, D., Melamed, M. L., and Gier, J.:
956 Fostering multidisciplinary research on interactions between chemistry, biology, and physics within the coupled
957 cryosphere-atmosphere system, Elementa-Science of the Anthropocene, 7, ARTN 58
958 10.1525/elementa.396, 2019.

959 Thornton, J. A., Kercher, J. P., Riedel, T. P., Wagner, N. L., Cozic, J., Holloway, J. S., Dube, W. P., Wolfe, G. M.,
960 Quinn, P. K., Middlebrook, A. M., Alexander, B., and Brown, S. S.: A large atomic chlorine source inferred from mid-
961 continental reactive nitrogen chemistry, Nature, 464, 271-274, 10.1038/nature08905, 2010.

962 Tokumasu, K., Harada, M., and Okada, T.: X-ray fluorescence imaging of frozen aqueous NaCl solutions, Langmuir,
963 32, 527-533, 10.1021/acs.langmuir.5b04411, 2016.

964 Wagner, R., Möhler, O., Saathoff, H., Schnaiter, M., and Leisner, T.: New cloud chamber experiments on the
965 heterogeneous ice nucleation ability of oxalic acid in the immersion mode, Atmos. Chem. Phys., 11, 2083-2110,
966 10.5194/acp-11-2083-2011, 2011.

967 Wagner, R., Mohler, O., and Schnaiter, M.: Infrared optical constants of crystalline sodium chloride dihydrate:
968 Application to study the crystallization of aqueous sodium chloride solution droplets at low temperatures, J Phys Chem
969 A, 116, 8557-8571, 10.1021/jp306240s, 2012.

970 Wagner, R., Höhler, K., Möhler, O., Saathoff, H., and Schnaiter, M.: Crystallization and immersion freezing ability of
971 oxalic and succinic acid in multicomponent aqueous organic aerosol particles, Geophys. Res. Lett., 42, 2464-2472,
972 10.1002/2015GL063075, 2015.

973 Waldner, A., Artiglia, L., Kong, X., Orlando, F., Huthwelker, T., Ammann, M., and Bartels-Rausch, T.: Pre-melting and
974 the adsorption of formic acid at the air–ice interface at 253 K as seen by NEXAFS and XPS, Phys. Chem. Chem. Phys.,
975 20, 24408-24417, 10.1039/C8CP03621G, 2018.

976 Wang, S., Schmidt, J. A., Baidar, S., Coburn, S., Dix, B., Koenig, T. K., Apel, E. C., Bowdalo, D., Campos, T. L.,
977 Eloranta, E., Evans, M. J., DiGangi, J. P., Zondlo, M. A., Gao, R.-S., Haggerty, J. A., Hall, S. R., Hornbrook, R. S.,
978 Jacob, D., Morley, B., Pierce, B., Reeves, M., Romashkin, P., ter Schure, A., and Volkamer, R.: Active and widespread
979 halogen chemistry in the tropical and subtropical free troposphere, Proc. Nat. Acad. Sci., 112, 201505142-201509286,
980 10.1073/pnas.1505142112, 2015.

981 Wise, M. E., Martin, S. T., Russell, L. M., and Buseck, P. R.: Water uptake by NaCl particles prior to deliquescence and
982 the phase rule, Aerosol Sci. Technol., 42, 281-294, 10.1080/02786820802047115, 2008.

983 Wise, M. E., Baustian, K. J., Koop, T., Freedman, M. A., Jensen, E. J., and Tolbert, M. A.: Depositional ice nucleation
984 onto crystalline hydrated NaCl particles: A new mechanism for ice formation in the troposphere, Atmos. Chem. Phys.,
985 12, 1121-1134, 10.5194/acp-12-1121-2012, 2012.

986 Wren, S. N., Donaldson, D. J., and Abbatt, J. P. D.: Photochemical chlorine and bromine activation from artificial saline
987 snow, Atmos. Chem. Phys., 13, 9789-9800, 10.5194/acp-13-9789-2013, 2013.

988 Yang, X., Neděla, V., Runštuk, J., Ondrušková, G., Krausko, J., Vetráková, Ľ., and Heger, D.: Evaporating brine from

989 frost flowers with electron microscopy and implications for atmospheric chemistry and sea-salt aerosol formation,

990 Atmos. Chem. Phys., 17, 6291-6303, 10.5194/acp-17-6291-2017, 2017.

991

992 **Appendix A**
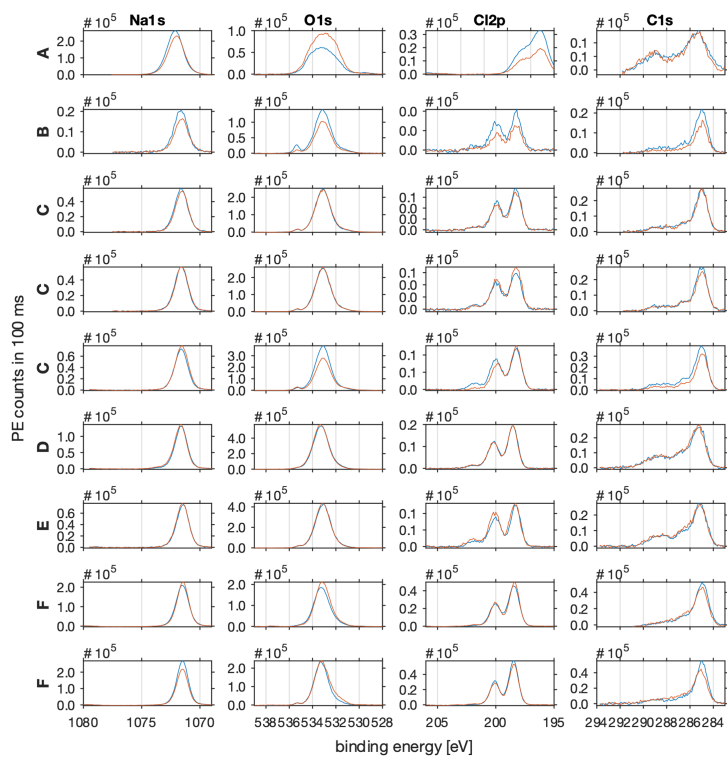
993

994 **Figure A1:** It shows the photo emission intensities as acquired before (blue line) and after (red
995 line) each NEXAFS spectrum. The PE spectra of sodium (Na1s) are shown in column 1, of oxygen
996 (O1s) in column 2, of chlorine (Cl2p) in column 3, and of carbon (C1s) in column 4. All spectra
997 were acquired at the Phoenix beam line of SLS of PSI with a photon energy of 2200 eV. Pass
998 energy was set to 100 eV and dwell time to 100 ms. Beam line slits were 2 x 2 mm. The C-H
999 feature at 285 eV of the C1s photoemission spectra served as binding energy reference and all
1000 spectra were shifted by 4-5.5 eV to account for charging effects.

1001

1002 The spectra in Fig. A1 can be described as follows:

1003 - The Na1s region shows one gauss-shaped feature at 1072 eV as expected for sodium.
1004 - The O1s region shows one dominant feature at 535 eV in line with oxygen in ice and a smaller feature at higher
1005   binding energy which might be attributed to gas-phase water.
1006 - The Cl2p region shows the typical doublet of the p-orbital spin-orbit splitting (p(3/2) and p(1/2)), 1.6 eV apart
1007   at 200 eV binding energy. Additionally, in some spectra a small feature at 203 eV binding energy is evident
1008   which might be attributed to the Cl2p(1/2) of organic carbon species.
1009 - The C1s region shows a broad spectrum with the main feature at 285 eV binding energy, typical for the C-H of
1010   adventitious carbon. The overlapping features at higher binding energy can be attributed to C-OH, C=O,
1011   C(O)=O and C-Cl.
1012 - The spectra of all species acquired before and after the sample in Figure A are significantly wider compared to
1013   the other samples. Additionally, the Cl2p features are shifted by 2 eV to lower binding energy. This sample is,
1014   unlike the others, is characterised by a large variation in sample thickness (Figure 3A of manuscript) which
1015   leads to differential charging and might explain the wider peak shapes and shift in the Cl2p features.
1016 - In sample A, the photoemission intensities of the Na1s and Cl2p show a higher intensity after the NEXAFS
1017   spectrum was acquired compared to before. During that time, the photoemission intensity of O1s increased.
1018   This suggests that water kept adsorbing to the sample and masked the signal intensity of the underlying sodium
1019   chloride.
1020 - In sample B, all photoemission intensities decreased during the time it took to acquire the NEXAFS spectra.
1021   This suggests that the working distances changed which impacts the sensitivity of all sample components.

1022

1023 **Appendix B**

1024 Freezing point depression data of NaCl (Rumble, 2019)

1025

mass fraction [%]	molal concentration [mol kg-1]	molar concentration [mol l-1]	freezing depression [K]
0.1	0.017	0.017	0.06
0.2	0.034	0.034	0.12
0.3	0.051	0.051	0.18
0.4	0.069	0.069	0.24
0.5	0.086	0.086	0.3
1	0.173	0.172	0.59
1.5	0.261	0.259	0.89
2	0.349	0.346	1.19
2.5	0.439	0.435	1.49
3	0.529	0.523	1.79
3.5	0.621	0.613	2.1
4	0.713	0.703	2.41
4.5	0.806	0.793	2.73
5	0.901	0.885	3.05
6	1.092	1.069	3.7
7	1.288	1.256	4.38
8	1.488	1.445	5.08
9	1.692	1.637	5.81
10	1.901	1.832	6.56
11	2.115	2.029	7.35
12	2.333	2.229	8.18

13	2.557	2.432	9.04
14	2.785	2.637	9.94
15	3.02	2.845	10.89
16	3.259	3.056	11.89
17	3.505	3.27	12.94
18	3.756	3.486	14.04
19	4.014	3.706	15.22
20	4.278	3.928	16.46
21	4.548	4.153	17.78
22	4.826	4.382	19.18
23	5.111	4.613	20.67

1026